International Journal of Material Forming (2024) 17:18
https://doi.org/10.1007/s12289-024-01820-4

ORIGINAL RESEARCH

Laser metal deposition of titanium on stainless steel with high powder flowrate for high interfacial strength

Di Cui[1] · Akash Aggarwal[1] · Marc Leparoux[1]

Received: 2 February 2024 / Accepted: 22 February 2024

Abstract
Direct joining of titanium and stainless steel 316 L with a strong interface is very challenging due to the formation of the brittle intermetallic compounds FeTi and Fe_2Ti in the intermixing zones and to the high residual stress induced by the mismatch of the thermal expansion coefficients. In this bimetallic directed energy deposition study, firstly, deposition of Ti on stainless steel was carried out using conventional process parameter regime to understand the interfacial cracking susceptibility and then a novel high powder flowrate approach is proposed for controlling the dilution and constraining the intermetallic phases forming at the interface. The influence of high temperature substrate preheating (520 °C) on the cracking susceptibility and interface strength was also investigated. The deposited Ti samples and their interfaces with the 316 L substrate were characterized with optical microscopy, scanning electron microscopy and energy dispersive X-ray spectroscopy to investigate the geometry, microstructures and chemical compositions in relation to the cracks. The high powder flowrate deposition of Ti on stainless steel 316 L results in an extremely thin dilution region (~ 10 µm melt pool depth in the substrate) restricting the formation of the intermetallic phases and cracks. The ultimate shear strength of the interfaces of the crack free sample was measured from cuboid deposits and the highest measured strength is 381 ± 24 MPa, exceeding the weaker base material pure Ti. The high interfacial strength for high powder flowrate deposition is due to the substantial attenuation and shadowing of the laser beam by the in-flight powder stream as demonstrated by the high-speed imaging resulting in an extremely small dilution region.

Keywords Laser metal deposition · Dissimilar joining · 316L SS – Ti system · Intermetallic compounds · Laser beam attenuation

Introduction

Titanium and its alloys are considered key engineering materials thanks to their outstanding combination of high strength-to-weight ratio, superior heat and corrosion resistance and biocompatibility [1–5]. Therefore, Ti (-alloys) have been considered excellent engineering materials in biomedical, aerospace, automobile, nuclear and many other industries [6–8]. However, the high cost and difficult machining of Ti (-alloys) limits their application. To combine the excellent properties of Ti (-alloys) and good formability, economic prices and other advantages of other alloys, the need of joining Ti (-alloys) with dissimilar metals for wider applications have arisen [9–11]. Stainless steels (SS) are more economic engineering materials with excellent corrosion resistance and mechanical properties. By manipulating the part design, dissimilar joining of Ti (-alloys) and SS can provide combined advantages for novel applications in various industries.

Joining of Ti (-alloys) and SS has been attempted with many techniques. In direct joining of these dissimilar materials, brittle intermetallic compounds (IMCs) like Fe_2Ti and FeTi form in the interfacial region [12, 13]. As most joining techniques involve heating and cooling, the mismatch between the coefficients of thermal expansion (CTE) of the base materials drastically increases the thermal stress and residual stress at the joint [14–16]. When cooled down from an elevated temperature, the CTE mismatch between two materials can induce tensile or compressive stress at the

✉ Marc Leparoux
marc.leparoux@empa.ch

[1] Laboratory for Advanced Materials Processing, Empa-Swiss Federal Laboratories for Materials Science and Technology, Feuerwerkerstrasse 39, Thun CH-3602, Switzerland

Published online: 04 March 2024

interface. Cracking and buckling can happen under these stress conditions, respectively. As a result of the mechanical and metallurgical factors, cracks are easily formed in the IMCs in the interfacial region, and quickly lead to failure of the joint. Laser welding has been applied to weld various alloy pairs [1, 9, 17–19]. Chen et al. used a continuous wave CO_2 laser to weld Ti-6Al-4 V and SS 201 plates [20]. When the laser beam was centered on the Ti-Fe interface, continuous distribution of large amount of Ti-Fe IMCs occurred in the weld seam, leading to poor ultimate tensile strength (UTS) of only 65 MPa. Offsetting the laser beam by 0.6 mm toward the SS created IMCs with uniform thickness of around 30 µm along the interface and improved the UTS to 150 MPa.

Directed energy deposition (DED) is an additive manufacturing (AM) technology capable of directly producing dense metal parts with complex geometry and especially varying composition. Among the different DED approaches, the Laser Metal Deposition (LMD) process is using a laser as heat source and metal powders as feeding material. The laser beam is focused on a metal substrate to create a melt pool, where a co-axially or laterally fed powder jet is also focused on. The metal powder is heated by the laser and normally melts in the melt pool and solidifies rapidly. Movement of the laser head and substrate can be controlled by a computer numerical control (CNC) system. The laser head and substrate move according to pre-defined route pattern to deposit the 3D work piece. LMD has unique advantages in depositing dissimilar materials within a single work piece. LMD of Ti (-alloys) and steels was first explored by Sahasrabudhe et al. [21]. Direct deposition of Ti64 (Ti-6Al-4) on SS 410 and compositionally graded SS 316 to Ti64 both failed due to extensive cracking. On one hand, large amounts of IMCs like Cr_2Ti, FeTi and Fe_2Ti were found in the interface. On the other hand, the thermal stress developed in SS 316 was calculated to be approximately four times as much as that in Ti64 without assuming any other phase formation. Li et al. also reported that the deposited SS 316 layer directly fell off from the Ti-6Al-4 V substrate with clear cracking sound during LMD [6]. Rashkovets et al. [22] tried the same process with different parameters and obtained less disastrous results, but still observed cracks at the interface. Cracking was likely due to the thermal stress and high temperature gradient during the cooling phase. To avoid the mixing of Ti (-alloys) and SS, interlayer of a third metal/alloy has been applied between the base materials. Such techniques either produce an interface with poor strength or involves toxic filler material like V and Cr [23–25].

To the best knowledge of the authors, defect free direct deposition of Ti (-alloy) on 316 L through LMD process has not yet been successful. To bridge this research gap, this study aims to enhance the interfacial strength and mitigate the crack formation by tailoring the extent of dilution and the subsequent formation of intermetallic phases. As the ratio of melted substrate and powder materials can be conveniently controlled with LMD parameters, it is promising to obtain metallurgical bonding between the base materials with proper interfacial composition and phases. Therefore, LMD has been studied in detail in this work with emphasis on the interface cracking, microstructure formation, intermetallic compounds, interface strength, and the laser beam attenuation to tackle the cracking problem when directly joining Ti (-alloys) and SS.

Materials and methods

Materials

150×150 mm^2 stainless steel 316 L plates with a thickness of 4 mm (HABA AG, Cham, Switzerland) were used as substrate. Commercially pure Cp-Ti grade 1 powder (AP&C Advanced Powders & Coatings Inc., Quebec, Canada) with a particle size distribution of 45–106 µm was used. The chemical compositions of the powder conform with the ASTM B348 standard. The powder particles are highly spherical and have few satellites or voids.

LMD system and experiments

A commercial LMD machine BeAM Mobile 1.0 (BeAM Machines, Strasbourg, France) equipped with a continuous wave (CW) 1068 nm Ytterbium fiber laser and a coaxial nozzle was used to deposit the Ti powder on the 316 L substrate. Further details of the machine can be found in previous studies [13, 26]. A hot plate (Fisherbrand Isotemp, Fisher Scientific AG, Reinach, Switzerland) was used in some cases for preheating the 316 L substrate. The LMD process was conducted under argon atmosphere (Ar 4.8, 99.998%) with O_2 and H_2O concentrations in the range of 1.0–10.0 ppm and 50.0-300.0 ppm, respectively. The main processing parameters are laser power (LP), powder flowrate (PF), and nozzle velocity (NV). According to the manufacturer, the reference parameters for Ti bulk deposition are LP = 325 W, PF = 4 g/min and NV = 2000 mm/min. For 316 L bulk deposition, the reference parameters are LP = 250 W, PF = 5 g/min and NV = 1000 mm/min. In this work, initially, single tracks were deposited with reference parameter regime on 316 L to investigate the influence on interface and geometry. Later, as shown in Sect. 3, a high nozzle traversal speed with high powder flowrate approach is proposed for controlling the dilution and constraining the IMCs forming at the interface. Then, Ti single layers were deposited with selected parameters developed from the proposed new strategy as

the foundation for subsequent cuboids on top. The single layer and cuboid samples produced without preheating are denoted as RT samples. The samples produced with the substrate preheated to 520 °C are denoted as HT samples. The HT samples were kept at 520 °C for another 1 h after the deposition finished, and cooled down at a stepped rate of 25 °C/5 min to room temperature.

Characterizations

A manual and an automatic cutting machine (Discotom-2 and Accutom-5, Struers GmbH, Birmensdorf, Switzerland) were used with Alu-Oxide cut-off wheels to cut the samples for cross-sections. A three-component resin Technovit® 4000 (Kulzer GmbH, Wehrheim, Germany) was used to embed the samples. The embedded samples were ground with SiC grinding papers up to 2500 grit. They were then polished with 6 and 3 µm diamond pastes, and finally with an oxide polishing suspension (OPS) solution (0.04 µm SiO_2 with 10% H_2O_2). The crystallographic and chemical features were investigated using an optical microscope (ZEISS Axioplan, Munich, Germany), a high-resolution SEM (Mira Tescan 3, Brno, Czech Republic) and an EDS detector (EDAX, Mahwah, NJ, USA) mounted in the Mira Tescan 3. The shear tests of the cuboid samples were performed on a shear tester (Electronic Digimess 1000, Walter + Bai AG, Löhningen, Switzerland) at a strain rate of 2.4 mm/min. The pressure head was set just above the first interfacial layer. The fracture surface of the samples after shear tests were observed with SEM. EDS point analyses and line scans were performed on the surfaces to obtain chemical composition.

High-speed imaging was carried out to visualize the influence of powder flowrate on the Gaussian beam attenuation and shadowing. For this purpose, an imaging setup consisting of a high-speed camera (Motion Pro Y4, Videal, Switzerland) with a microscopic telecentric lens (ML-Z07545, Moritex, Japan) and a LED based illumination system was used to capture the in-flight powder stream – laser beam interaction. The imaging was carried out with a frame rate of 7.33 kHz, exposure time of 31 µs, image size of 544 × 708 pixels, and 8-bit pixel depth. The powder stream imaging was carried out for two different powder flowrates: In the first case, the powder flowrate (PF) was 2.5 g/min and in the second case, the PF was 21 g/min. For both the cases, the laser power was 250 W, and the nozzle head was stationary.

Results

Interfacial zone in the standard deposition regime

Ti single tracks were deposited directly on 316 L by varying the process parameters around the reference printing parameters for titanium. Thus, the laser power varied from 175 to 350 W, the nozzle velocity from 700 to 1400 mm/min and the powder flowrate from 2.5 to 5 g/min. Figure 1 shows, for example, the cross-section of a single track deposited using LP = 175 W, NV = 1000 mm/min and PF = 2.5 g/min. Many cracks are observed on the top surface. A few large spherical (diameter around 100 µm) and smaller non-spherical

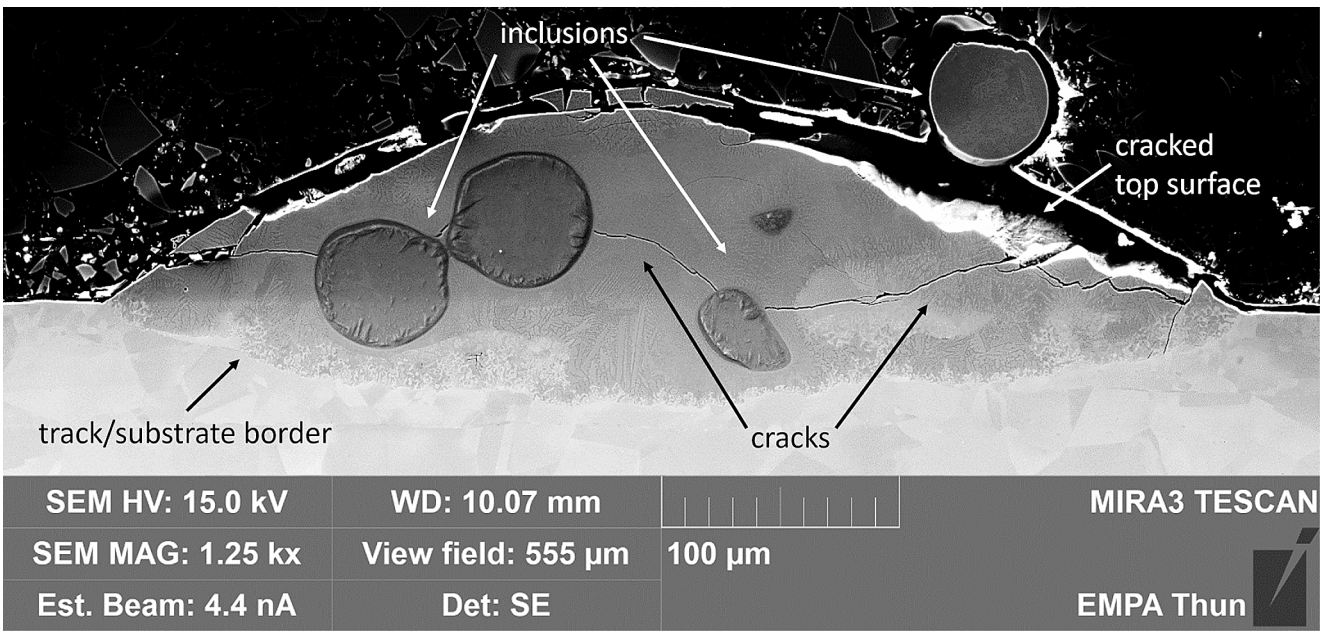

Fig. 1 SEM image of the cross-section of a Ti single track deposited on stainless steel 316 L in the standard processing regime

inclusions are observed in the track. Cracks run through the track but do not penetrate into the inclusions or the substrate. The interface can be clearly seen between the track and the substrate material.

Microstructure has been observed under a SEM and the composition has been analyzed by EDS. For simplification, only the ratio of Fe and Ti is considered until further detailed discussions. The different regions observed on the cross-sections from the stainless steel substrate to the top surface of the Ti deposit are represented for instance in Fig. 2.

The equiaxed area at the bottom shows an atomic composition of $Fe_{79}Cr_{19}Ni_{10}$, conforming to the chemical composition of the substrate material 316 L. The composition in this area is denoted as Fe100. A dark sphere with a diameter of around 50 µm is seen at the top left. Its composition is pure Ti, denoted as Fe0. Therefore, the dark sphere and other similar objects are estimated to be partially melted Ti particles. Four interfacial regions with complex microstructures can be distinguished between the pure Ti and 316 L. Region I is the closest to 316 L. It is a reticular region with white, grey and dark structures showing different compositions. The dendritic Region II has dendrites with higher Fe concentration than the interdendritic areas. Region III has a dark matrix and small precipitates. Region IV has a dark matrix with very low Fe concentration of Fe ~ 22 and network precipitates. All these four regions contain at least one intermetallic compound and the compositions could be correlated to the different phases described in the Fe-Ti phase diagram in Fig. 3.

The variation of the process parameters around the conditions used typically for depositing Ti in a LMD process showed no significant modification of the above-described phases and, in particular, a large interface of a few tens of microns containing the intermetallics was always observed.

Control of the interfacial zone using the high powder flowrate regime

As no satisfying conditions could be identified within the conventional processing windows, a new strategy has to be proposed. Considering the 2D geometry of the single-track cross-sections, different dimensions have been considered for characterizing the interfacial zone. The penetration depth D is the depth of the solidified melt pool below the surface of the substrate. The added height H is the height of the deposited material above the surface of the substrate. The melt pool width W is the width of the melt pool at the level of the surface of the substrate. These features are marked on schematic of a single-track cross-section in Fig. 4. The ratio H/W is denoted as aspect ratio AR. Additionally, the dilution term (D_L) is defined as the ratio of the melt pool area (A_m) in the substrate to the sum of the melt pool area and the clad deposit area (A_d), calculated as $D_L = A_m/(A_m + A_d)$.

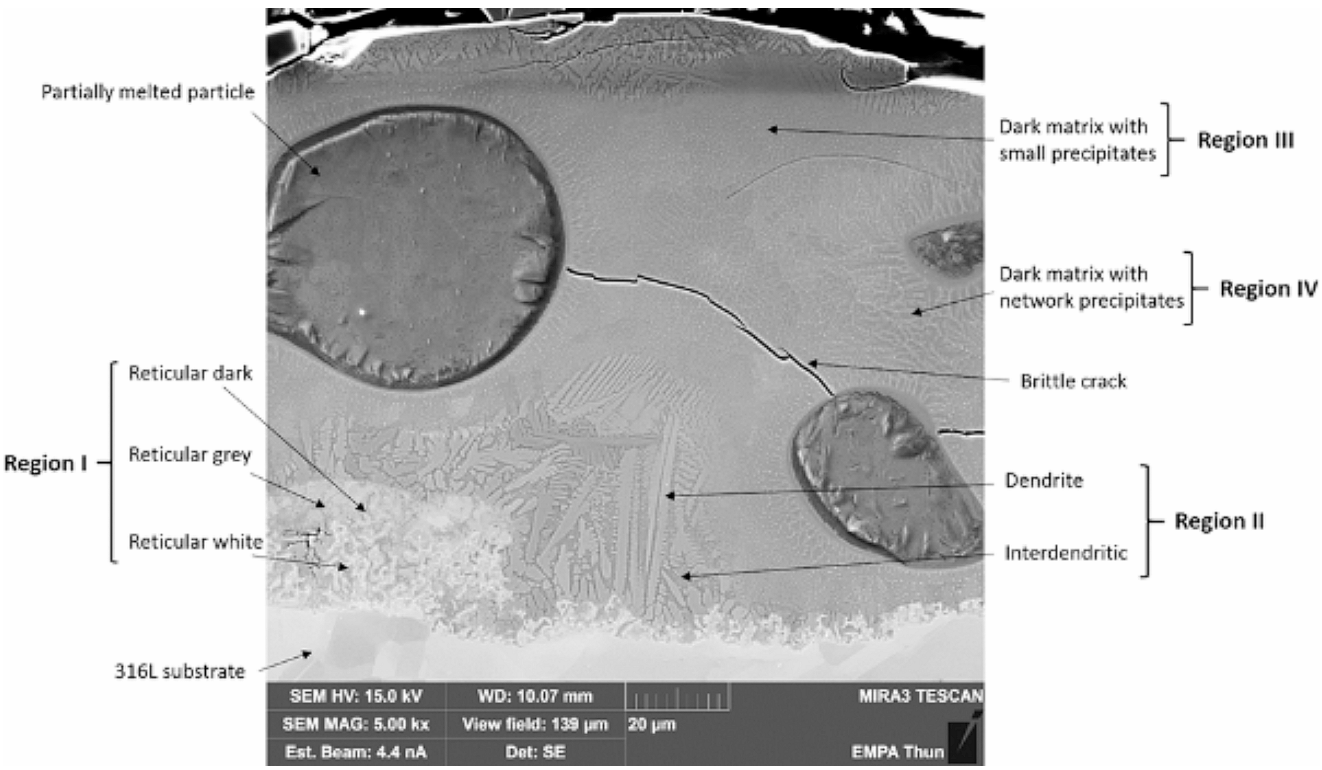

Fig. 2 Different regions marked in the Ti single track with their microstructures

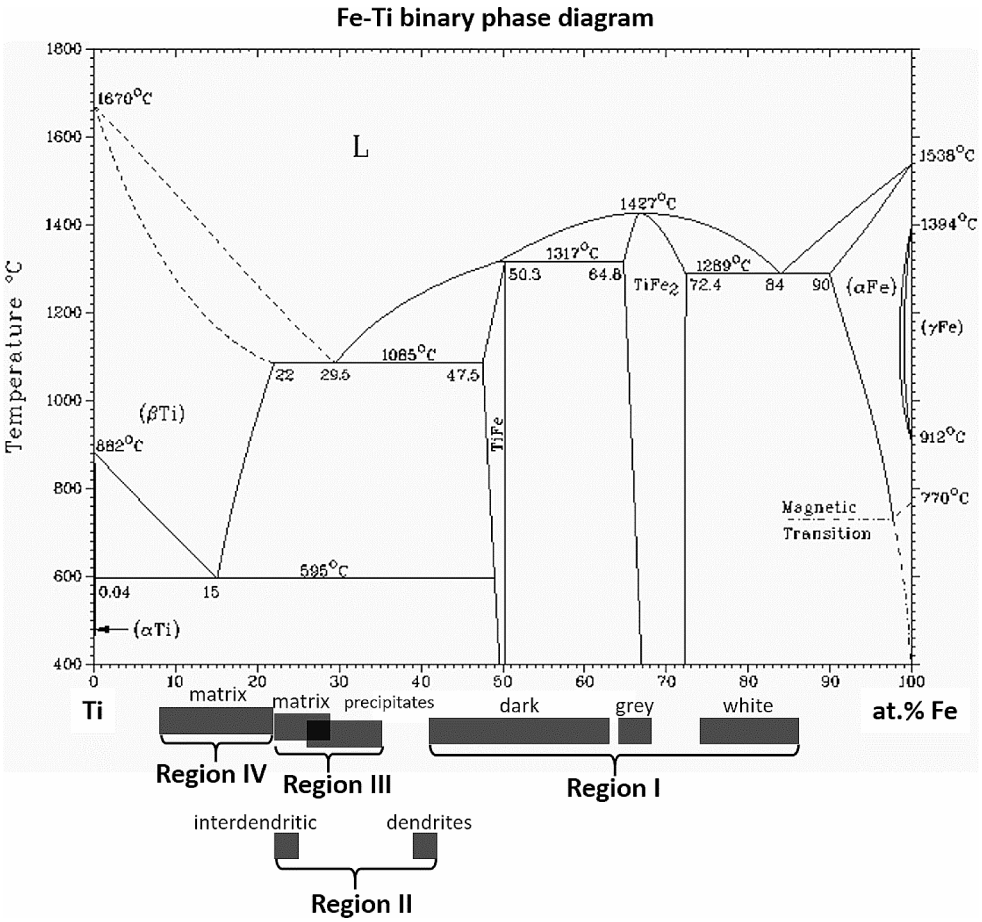

Fig. 3 The range of Fe atomic percentage in the features in the reaction regions I, II, III and IV marked on the Fe-Ti binary phase diagram

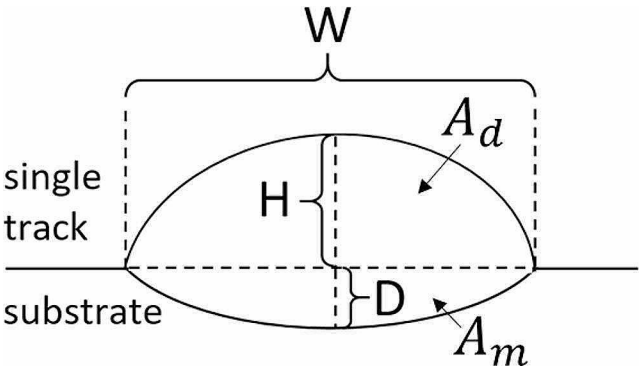

Fig. 4 Schematic of a single-track cross-section. The penetration depth (D), deposited height (H), width (W), melt pool area (A_m) in the substrate, and clad deposit area (A_d) are marked

For avoiding an extensive formation of intermetallics, the dilution has to be minimized. Nevertheless, a certain penetration depth is required for achieving a sufficient mechanical bonding at the interface. The deposited height should be also sufficient to prevent damaging the interfacial zone during the deposition of the subsequent layer on the top. Finally, during building a 3D part, an overlap of the tracks is performed. A high aspect ratio, meaning a high contact angle between the track and the substrate could induce inter-track voids. Thus, the aspect ratio should be also controlled.

Table 1 Parameters for single tracks showing the effect of entering the high PF regime

Group	Sample No.	LP (W)	NV (mm/min)	PF (g/min)
M	1	250	700	2.5
	2	250	700	21
	3	250	13,000	21
	4	500	13,000	21

First, high powder flowrates should actually allow having a low dilution. Second, a high nozzle velocity would help reducing the height of the deposit and avoiding too large contact angles. It should be noted that the NV should not be so high that the deposit has a too small height to protect the first interface from subsequent deposition on top of the first layer. Finally, due to the high particle density in the powder jet, the laser power has to be also scaled up to melt the larger amount of powder material.

Thus, Ti single tracks were deposited to study the effect of entering the high PF regime from the typical process window. The investigated parameters aiming to control dilution are summarized in Table 1.

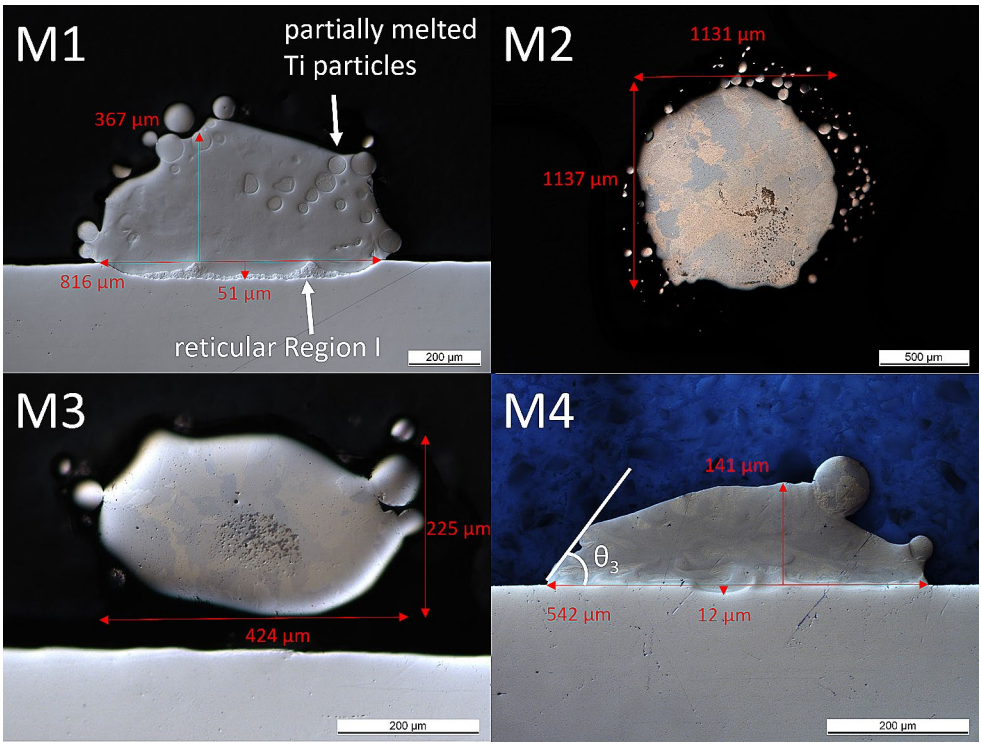

Fig. 5 The OM images of the cross-section of the M group single tracks. The acute contact angle in M4 is marked as θ_3

Table 2 Parameters for the Ti single layers. Reference parameters for the Ti cuboids on top are in the last row

Group	Sample No.	LP (W)	NV (mm/min)	PF (g/min)	HS (mm)	ΔZ (mm)
Pd	3	450	9000	32	0.459	-
Pe	4	500	13,000	32	0.425	-
	5	500	20,000	32	0.392	-
Fc	5	500	20,000	14	0.358	-
Fd	3	500	9000	21	0.500	-
	4	500	13,000	21	0.431	-
Cuboid	-	325	2000	4	0.500	0.200

Typical cross-sections of these tracks are shown in Fig. 5. Track M1 was deposited with parameters in the typical range for LMD for comparison and has a normal track geometry with a penetration depth D of 51 µm. A reticular Region I is observed at the bottom of the solidified melt pool. Several partially melted particles and cracks are observed in the deposition. Track M2 was deposited with significantly increased PF compared to M1. M2 detached from the substrate immediately. Its cross-section in Fig. 5 is nearly a circle with a diameter of around 1100 µm. No trace of penetration was observed on the substrate side. Track M3 was deposited with significantly increased NV compared to M2. M3 has a much smaller cross-section (an area of 9.3×10^4 μm^2) than M2 (an area of 1.0×10^6 μm^2). M3 does not bond with the substrate either. Track M4 was deposited with doubled LP comparing to M3. M4 bonds to the substrate with a very small penetration depth D of 12 µm maximum. The track forms an acute contact angle with the substrate.

Based on the above-mentioned results, 2-dimensional single layers were deposited with parameters varying around the conditions for printing the M4 structure. On top of these interfacial layers, Ti cuboids ($5\times5\times3$ mm^3) were printed using standard processing parameters. These parameters are summarized in Table 2. For all of these process parameters, the printing is carried out without preheating (denoted as RT samples) as well as substrate preheating of 520 °C (denoted as HT samples). The hatch spacing (HS) was selected as 75% of the measured width of each single track.

All single interfacial layers showed a good adherence to the 316 L substrate but many cuboid samples delaminated at the interface after mechanical cutting. The samples produced with the Fd_4 parameter set were further investigated as an example.

The OM images of the Ti-316 L interface in single layer RT_Fd_4, cuboid RT_Fd_4, single layer HT_Fd_4 and cuboid HT_Fd_4 are shown in Fig. 6. Layers RT_Fd_4 and HT_Fd_4 both show a good adherence to the substrate.

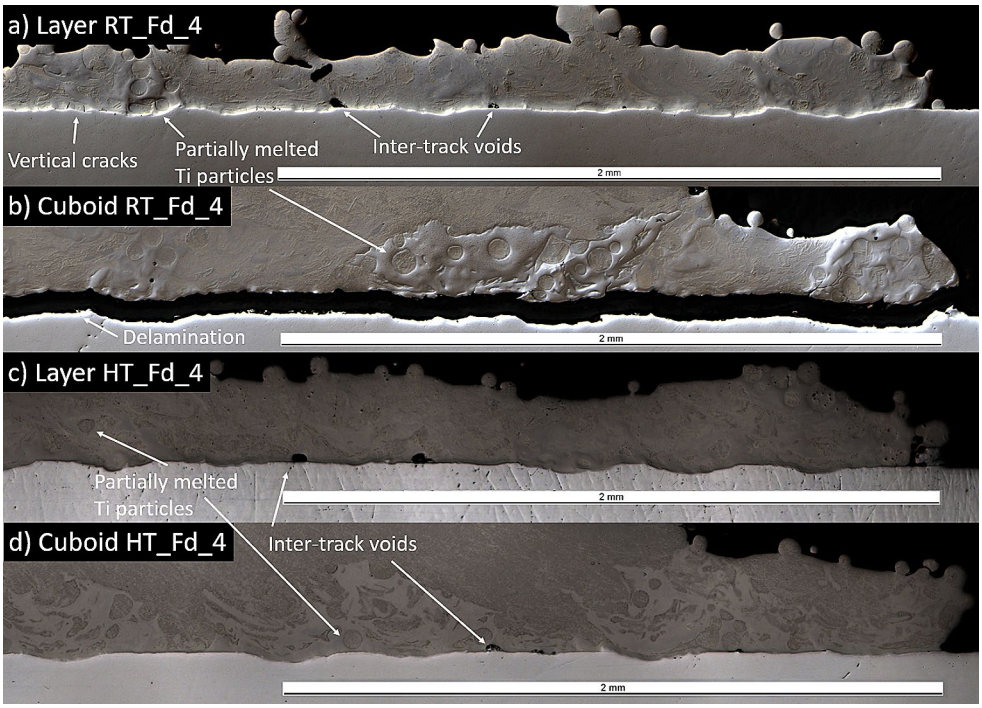

Fig. 6 OM images of the Ti-316 L interface in (a) single layer RT_Fd_4, (b) cuboid RT_Fd_4, (c) single layer HT_Fd_4 and (d) cuboid HT_Fd_4.

Some small vertical cracks are however observed in RT_Fd_4. Cuboid RT_Fd_4 delaminated from the substrate at the interface, while the preheated HT_Fd_4 shows a good adherence with the substrate. Partially melted Ti particles and inter-track voids are observed in the first layer in almost all samples.

Interfacial strength

The interfacial strength was measured by shear testing five identical cuboid specimens. The specimens were cut with EDM to particularly avoid inflicting crack initiation at the cross-sections. The pressure head of the shear tester was positioned just above the first interfacial layer.

The maximum shear force F_{max} and delaminated surface area A were obtained for each sample and fall in ranges of 3166 ~ 9150 N and 24 ~ 70 mm^2, respectively. The ultimate shear strength (USS) is calculated as $USS = F_{max}/A$ and summarized in Fig. 7. The USS of the RT samples are in a range of 45 ~ 153 MPa. The HT samples have significantly higher USS in a range of 173 ~ 381 MPa. The interface in HT_Fd_4 cuboids have the highest USS of 381 ± 24 MPa, higher than the weaker base material pure Ti (371 MPa [27]) and lower than 316 L (517 MPa [28]).

Discussion

In the LMD process, Ti is mixed with 316 L in the liquid state and the mixture forms complex microstructures in the solidified melt pool. The SEM image of track PF2_1 in Fig. 2 demonstrates the four reaction regions between the 316 L substrate and the pure Ti regions. The composition in the reaction regions covers a large range in the Fe-Ti phase diagram. At least, the two brittle IMCs, Fe_2Ti and FeTi, form in the deposit during the solidification process and easily lead to cracks. In order to reduce the risk of cracking at the interface, all of the four reaction regions have to be reduced so that the brittle IMCs are constrained within only a thin interfacial region. This is achievable by reducing the dilution of the substrate material into the melt pool. During the LMD process, the laser beam first hits the focused powder jet. Part of the laser energy is absorbed and reflected by the powder jet, and the transmitted part is used to heat and melt the substrate. Therefore, the dilution can be substantially reduced by increasing the powder flowrate resulting in significant attenuation of the laser beam. The increase in the laser beam attenuation for high PF can be understood with the high-speed imaging of the powder stream. Figure 8 shows the interaction of the laser beam with the in-flight powder particles for powder flowrate of 2.5 g/min (Fig. 8b) and 21 g/min (Fig. 8c). In the coaxial LMD process, the inner portion of the powder stream interacts with the laser beam resulting in absorption, attenuation and shadowing of the beam. These particles (glowing) with high thermal energy can be clearly seen in Fig. 8b (PF = 2.5 g/min) and

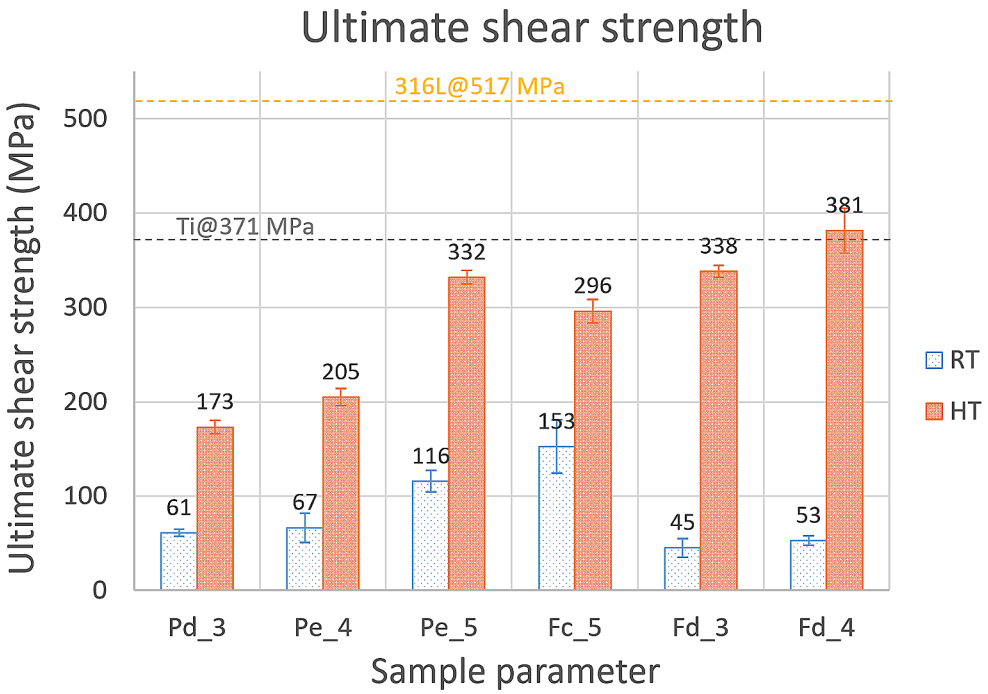

Fig. 7 The ultimate shear strength measured from the cuboid samples

Fig. 8c (PF = 21 g/min). The extent of laser beam attenuation directly depends on the powder flowrate. As shown in Fig. 8b and c, the number of glowing particles is smaller for PF of 2.5 g/min which results in low attenuation of the laser beam, whereas, as shown by the strength of the glowing region in Fig. 8c, the attenuation of the laser beam is extremely high for PF of 21 g/min due to the interaction of large number of particles with the laser beam. This extremely high attenuation of laser beam for high powder flowrate results in a very low dilution depth.

Increasing only the PF significantly (from typically 2.5 g/min to 21 g/min) resulted in a thick cylindrical deposit M2 as shown in Fig. 5. Such a cross-section makes it impossible to deposit adjacent single tracks to form a dense 2-dimensional layer. Therefore, the nozzle velocity NV had to be increased to distribute the deposit material along the scanning direction and decrease the height of the deposit. M3, produced with both increased PF and NV shows improvement in the geometry of the cross-section but still no effective bonding with the substrate. Then, the laser power LP was also increased to produce sample M4, which has both a thin interfacial region of around 12 µm and an acute contact angle on the edges. The acute contact angle reduces the risk of forming inter-track porosity when adjacent tracks are deposited.

Ti single layers have been deposited directly on 316 L substrate with the optimal parameters selected from the high PF single track deposition experiments. The IMCs are generally constrained within thin interfacial regions as in the high PF single tracks. In the cuboid samples, the subsequent layers on top did not induce obvious changes in the first interface.

Although the parameters used to deposit the single layers were selected for avoiding inter-track voids, such defects have been observed periodically at the interface. This is estimated due to the relatively small process window. Overhanging structures might have formed in random locations in the scan direction on the edges of the single tracks during deposition of the full single layers and created the inter-track voids. Other defects like small vertical cracks in the two interfacial thin bands and partially melted Ti particles in the deposition are also observed in RT samples. Despite the presence of these defects, the single layer samples bond to the substrate after being cut mechanically for their cross-section. But when Ti cuboids are added on top of the single layers, most of the samples delaminated at the interface between the first layer and the substrate at the interface. This is a result of thermal stress generated over the many more thermal cycles and in larger volumes as the deposit goes from 2D layer to a 3D structure.

The ultimate shear strength USS of the RT samples are in a range of 45 ~ 153 MPa. This is already a great improvement compared with literature where the deposit directly fell off from the substrate during the LMD process [6]. Preheating of the substrate and controlled cooling (25 °C/5 min) after deposition led to almost crack free interfaces and further increased the USS of the interfaces. The HT samples have USS in a range of 173 ~ 381 MPa, with the highest strength of 381 ± 24 MPa exceeding pure Ti (USS = 371 MPa) but below SS316 (USS = 517 MPa).

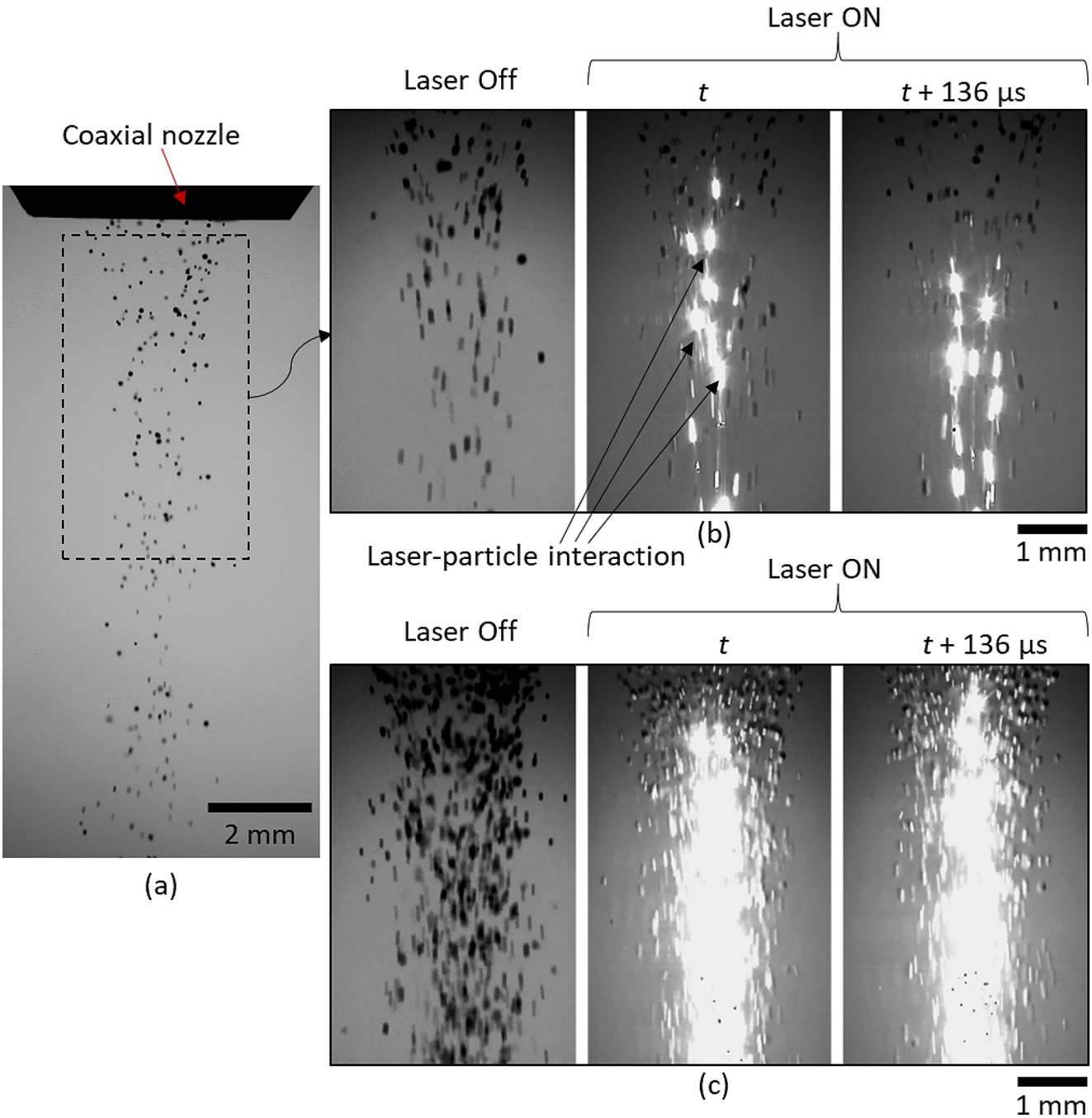

Fig. 8 (a) Powder stream spatial distribution measured by high-speed imaging. Visualization of laser-powder stream interaction resulting in Gaussian beam attenuation: (b) powder flowrate = 2.5 g/min, and (c) powder flowrate = 21 g/min

Substrate preheating is a commonly used method for mitigating distortion and reducing cracks [29, 30]. Preheating the substrate to 400 °C led to a reduction in residual stress by 40% in a study on LMD of SS 304 [31–33]. Figure 7 shows that the HT samples have significantly improved USS compared to their RT counterparts. Preheating and controlled cooling can benefit the interface in multiple aspects. FeTi has been found to be the main IMC phase in the interfacial regions. The brittle-to-ductile transition temperature of FeTi is reported in a range between 500 and 600 °C [34]. FeTi behaves in brittle manner below 500 °C and becomes ductile above 600 °C. For the HT samples in this study, the substrate was effectively preheated to 520 °C before deposition started. Given the continuous heat input of the deposition process, the temperature in the interfacial regions is estimated to be maintained in the ductile range of FeTi during the LMD process. In addition, the amplitude of temperature variation in the solid and the thermal gradient are reduced

due to elevated base temperature. Thermal stress due to CTE mismatch and cycles of thermal expansion and contraction is thus reduced. As a result, the risk of hot cracks during the LMD process is reduced thanks to preheating.

Conclusion

In this work, a novel high powder flowrate approach is proposed for improvement in the interfacial strength and mitigation of cracks during the directed energy deposition of titanium on stainless steel. It was found that the direct deposition with the optimized process parameter regime of Ti on stainless steel 316 L results in a significant dilution region leading to the formation of brittle intermetallic phases and cracks. At the interfacial region, 316 L substrate and Ti powder mix in the liquid state and forms various phases in different reaction regions. In order to reduce the crack formation, dilution and IMCs formation at the interface need to be controlled. The IMC regions should be as thin as possible for achieving a high interfacial strength. For this purpose, a special strategy based on laser attenuation is applied for controlling the interface. As demonstrated by the high-speed imaging of the in-flight powder stream, the extent of laser beam attenuation depends directly on the powder flowrate. Therefore, using high powder flowrate leads to substantially high laser beam attenuation, which results in an extremely small dilution region restricting the formation of the intermetallic phases and cracks, while maintaining an interfacial mechanical bonding. Using the high powder flowrate (PF) strategy for the interfacial layer, the melting depth of the substrate is as low as around 12 µm. In this way, the dilution of Fe from the substrate into the melt pool is limited to a very low extent. Ultimate shear strength (USS) of 45 ~ 153 MPa has been achieved. Furthermore, preheating of the substrate and controlled cooling at 25 °C/5 min after deposition reduced the risk of cracking during the LMD process and residual stress at room temperature. Standard deposition recipe can be applied for the subsequent 3D structure on top as the interfacial region is not changed anymore. With the thermal management, the USS of the interface has been improved to 173 ~ 381 MPa. The highest USS of the interface produced is 381 ± 24 MPa, exceeding the weaker base material pure Ti. The proposed high powder flowrate strategy can be transferred to dissimilar deposition of other material pairs where brittle IMCs can form, such as Ti(-alloys) with other steels, Inconel, Invar, CoCrMo, etc.

Funding Open Access funding provided by Lib4RI – Library for the Research Institutes within the ETH Domain: Eawag, Empa, PSI & WSL.

Declarations

Conflict of interest The authors declare that they have no conflict of interest.

References

1. Mannucci A, Tomashchuk I, Mathieu A, Cicala E, Boucheron T, Bolot R, Lafaye S (2018) Direct laser welding of pure Titanium to Austenitic Stainless Steel. Procedia CIRP 74:485–490. https://doi.org/10.1016/j.procir.2018.08.138
2. Lee MK, Lee JG, Lee JK, Hong SM, Lee SH, Park JJ, Kim JW, Rhee CK (2011) Formation of Interfacial Brittle Phases Sigma Phase and IMC in Hybrid Titanium-to-Stainless Steel Joint. Trans Nonferrous Met Soc China 21:7–11. https://doi.org/10.1016/S1003-6326(11)61051-0
3. Zhao Z, Tariq NulH, Tang J, Ren Y, Liu H, Tong M, Yin L, Du H, Wang J, Xiong T (2020) Influence of annealing on the microstructure and Mechanical Properties of Ti/Steel Clad Plates Fabricated via Cold Spray Additive Manufacturing and Hot-Rolling. Mater Sci Eng: A 775:138968. https://doi.org/10.1016/j.msea.2020.138968
4. Yang X, Shi C, Ge Y, Sabuj MNH (2018) Comparison of microstructure and Mechanical Properties of Titanium/Steel Composite Plates by two Manufacturing processes. J Iron Steel Res Int 25(3):347–356. https://doi.org/10.1007/S42243-018-0038-Y
5. Yang D, Luo Z, Xie G, Wang M, Misra RDK (2018) Effect of Vacuum Level on Microstructure and Mechanical properties of Titanium–Steel Vacuum Roll clad plates. J Iron Steel Res Int 25:72–80. https://doi.org/10.1007/s42243-017-0009-8
6. Li W, Yan L, Karnati S, Liou F, Newkirk J, Taminger KMB, Seufzer WJ (2017) Ti-Fe Intermetallics Analysis and Control in Joining Titanium Alloy and Stainless Steel by Laser Metal Deposition. J Mater Process Technol 242:39–48. https://doi.org/10.1016/j.jmatprotec.2016.11.010
7. Gilbert SM (2018) Solid-state joining of titanium alloy to stainless steel. Dissertation Colorado School of Mines
8. Kundu S, Chatterjee S (2011) Effects of temperature on interface microstructure and strength properties of titanium–niobium stainless steel diffusion bonded joints. Mater Sci Technol 27(7):1177–1182. https://doi.org/10.1179/026708309X12595712305870
9. Satoh G, Yao YL, Qiu C (2013) Strength and microstructure of laser fusion-welded Ti–SS dissimilar material pair. Int J Adv Manuf Technol 66:469–479. https://doi.org/10.1007/s00170-012-4342-6
10. Zhou Q, Liu R, Zhou Q, Fan K, Xie J, Chen P, Rittel D (2022) Tensile behavior of the titanium-steel explosive welded interface under quasi-static and high-strain rate loading. Int J Solids Struct 254–255. https://doi.org/10.1016/j.ijsolstr.2022.111870

11. Wu T, Yang C (2022) Influence of pulse TIG welding thermal cycling on the microstructure and mechanical properties of explosively weld titanium/steel joint. Vacuum 197:110817. https://doi.org/10.1016/j.vacuum.2021.110817
12. Loh GH, Pei E, Harrison D, Monzón MD (2018) An overview of functionally graded additive manufacturing. Additive Manuf 23:34–44. https://doi.org/10.1016/j.addma.2018.06.023
13. Cui D, Mohanta A, Leparoux M (2020) Interface Control in Additive Manufacturing of Dissimilar metals Forming Intermetallic Compounds-Fe-Ti as a Model System. Materials 13(21):4747. https://doi.org/10.3390/ma13214747
14. Onuike B, Bandyopadhyay A (2018) Additive Manufacturing of Inconel 718 – Ti6Al4V bimetallic structures. Additive Manuf 22:844–851. https://doi.org/10.1016/j.addma.2018.06.025
15. Special Metals Corporation : INCONEL® Alloy 718 product brochure, Publication Number SMC-045
16. Peters M, Kumpfert J, Ward CH, Leyens C (2003) Titanium alloys for Aerospace Applications. Adv Eng Mater 5:419–427. https://doi.org/10.1002/adem.200310095
17. Chen H-C, Pinkerton AJ, Li L (2011) Fibre Laser Welding of Dissimilar alloys of Ti-6Al-4V and Inconel 718 for Aerospace Applications. Int J Adv Manuf Technol 52:977–987. https://doi.org/10.1007/s00170-010-2791-3
18. Gao M, Wang ZM, Li XY, Zeng XY (2012) Laser keyhole welding of Dissimilar Ti-6Al-4V Titanium Alloy to AZ31B Magnesium Alloy. Metall Mater Trans A 43:163–172. https://doi.org/10.1007/s11661-011-0825-6
19. Chen H-C, Bi G, Lee BY, Cheng CK (2016) Laser welding of CP Ti to stainless steel with different temporal pulse shapes. J Mater Process Technol 231:58–65. https://doi.org/10.1016/j.jmatprotec.2015.12.016
20. Chen S, Zhang M, Huang J, Cui C, Zhang H, Zhao X (2014) Microstructures and mechanical property of laser butt welding of titanium alloy to stainless steel. Mater Design 53:504–511. https://doi.org/10.1016/j.matdes.2013.07.044
21. Sahasrabudhe H, Harrison R, Carpenter C, Bandyopadhyay A (2015) Stainless steel to titanium bimetallic structure using LENS™. Additive Manuf 5:1–8. https://doi.org/10.1016/j.addma.2014.10.002
22. Rashkovets M, Mazzarisi M, Nikulina AA, Casalino G (2020) Analysis of laser direct stainless steel powder deposition on Ti6Al4V substrate. Mater Lett 274:128064. https://doi.org/10.1016/j.matlet.2020.128064
23. Tomashchuk I, Sallamand P (2018) Metallurgical strategies for the joining of Titanium alloys with steels. Adv Eng Mater 20(6):1700764. https://doi.org/10.1002/adem.201700764
24. Sidambe AT (2014) Biocompatibility of Advanced Manufactured Titanium Implants-A Review. Materials 7(12):8168–8188. https://doi.org/10.3390/ma7128168
25. Wiegand M, Marks L, Sommer N, Böhm S (2023) Dissimilar micro beam welding of titanium to Nitinol and stainless steel using biocompatible filler materials for medical applications. Weld World 67:77–88. https://doi.org/10.1007/s40194-022-01412-3
26. Cui D, Lanfant B, Leparoux M, Favre S (2021) Additive Manufacturing of Ti-Nb Dissimilar metals by Laser Metal Deposition. In: Meboldt M, Klahn C (eds) Industrializing Additive Manufacturing. Springer International Publishing, pp 96–111. https://doi.org/10.1007/978-3-030-54334-1_8
27. Suryawanshi J, Singh G, Msolli S, Jhon MH, Ramamurty U (2021) Tension-compression asymmetry and shear strength of titanium alloys. Acta Mater 221:117392. https://doi.org/10.1016/j.actamat.2021.117392
28. Shear Strength Metal Specifications | UniPunch Tooling Systems. UniPunch. https://unipunch.com/support/charts/material-specifications/
29. Corbin DJ, Nassar AR, Reutzel EW, Beese AM, Michaleris P (2018) Effect of substrate thickness and preheating on the distortion of laser deposited Ti–6Al–4V. J Manuf Sci Eng 140(6):061009. https://doi.org/10.1115/1.4038890
30. Le Dantec MCL (2018) Additive Fabrication of Silicon Pillars on Monocrystalline Silicon by Direct Laser Melting. Dissertation EPFL, Lausanne
31. Vasinonta A, Beuth JL, Griffith M (2007) Process maps for Predicting residual stress and Melt Pool size in the laser-based fabrication of thin-walled structures. J Manuf Sci Eng 129(1):101–109. https://doi.org/10.1115/1.2335852
32. Yılmaz N, Kayacan MY (2021) Effect of single and multiple parts manufacturing on temperature-induced residual stress problems in SLM. Int J Mater Form 14(3):407–419. https://doi.org/10.1007/s12289-020-01560-1
33. He B, Bi C, Li X, Wang W, Yang G (2023) Residual stresses and deformations of laser additive manufactured metal parts: a review. Int J Mater Form 16(1):7
34. Suzuki T, Uehara S (1980) Mechanical properties of FeTi, CoTi, and NiTi at elevated temperatures. Titanium 2:1255–1263